



Review

Biospeckle Analysis and Biofilm Electrostatic Tests, Two Useful Methods in Microbiology

Emilia Oleandro ^{1,2}, Simonetta Grilli ¹, Romina Rega ¹, Martina Mugnano ¹, Vittorio Bianco ¹, Marika Valentino ^{1,3}, Biagio Mandracchia ¹, Filomena Nazzaro ^{4,*}, Raffaele Coppola ⁵ and Pietro Ferraro ¹

- ¹ Institute of Applied Sciences & Intelligent Systems, National Research Council (CNR-ISASI), Via Campi Flegrei 34, 80078 Pozzuoli, Italy; emilia.oleandro@isasi.cnr.it (E.O.); simonetta.grilli@isasi.cnr.it (S.G.); romina.rega@isasi.cnr.it (R.R.); martina.mugnano@isasi.cnr.it (M.M.); vittorio.bianco@isasi.cnr.it (V.B.); marika.valentino@isasi.cnr.it (M.V.); b.mandracchia@isasi.cnr.it (B.M.); pietro.ferraro@isasi.cnr.it (P.F.)
- ² Department of Mathematics and Physics, University of Campania “Luigi Vanvitelli”, Viale Abramo Lincoln, 5, 81100 Caserta, Italy
- ³ Department of Electrical and Information Technology Engineering, University of Naples “Federico II”, Via Claudio, 21, 80125 Napoli, Italy
- ⁴ Institute of Food Science, National Research Council (CNR-ISA), Via Roma 64, 83100 Avellino, Italy
- ⁵ Department of Agriculture, Environment and Food, University of Molise, Via de Sanctis snc, 86100 Campobasso, Italy; coppola@unimol.it
- * Correspondence: filomena.nazzaro@isa.cnr.it; Tel.: +39-0825-299102



Citation: Oleandro, E.; Grilli, S.; Rega, R.; Mugnano, M.; Bianco, V.; Valentino, M.; Mandracchia, B.; Nazzaro, F.; Coppola, R.; Ferraro, P. Biospeckle Analysis and Biofilm Electrostatic Tests, Two Useful Methods in Microbiology. *Appl. Microbiol.* **2021**, *1*, 557–572. <https://doi.org/10.3390/applmicrobiol1030036>

Academic Editor:
Joaquín Bautista-Gallego

Received: 21 September 2021
Accepted: 12 November 2021
Published: 17 November 2021

Publisher’s Note: MDPI stays neutral with regard to jurisdictional claims in published maps and institutional affiliations.



Copyright: © 2021 by the authors. Licensee MDPI, Basel, Switzerland. This article is an open access article distributed under the terms and conditions of the Creative Commons Attribution (CC BY) license (<https://creativecommons.org/licenses/by/4.0/>).

Abstract: The development of more sensitive methodologies, capable of quickly detecting and monitoring a microbial population present in a specific biological matrix, as well as performing to allow for the study of all its metabolic changes (e.g., during the formation of biofilm) to occur, is an essential requirement for both well-being and the food industry. Two techniques, in particular, have gained the attention of scientists: The first is “biospeckle”, an optical technique representing an innovative tool for applications in food quality, food safety, and nutraceuticals. With this technique, we can quickly evaluate and monitor the presence of bacteria (or their proliferation) in a solid or liquid biological matrix. In addition, the technique is helpful in quantifying and optimizing the correct storage time of the pro-biotics, if they are entrapped in matrices such as alginate and follow their survival rate in simulated gastro-intestinal conditions. A second technique with great chances is the “biofilm electrostatic test” (BET). BET undoubtedly represents a fast, simple, and highly reproducible tool suitable for admitting the evaluation of the in vitro bacterial capacity in order to adhere through an electrostatic interaction with a pyro-electrified carrier after only 2 h of incubation. BET could represent the way for a quick and standardized evaluation of bacterial resistance among biofilm-producing microorganisms through a fast evaluation of the potential presence of the biofilm.

Keywords: biofilms; probiotics; optical techniques; BET carrier; pyro-electrified polymer sheets; bacterial adhesion; food quality and safety; health

1. Introduction

Bacteria are present in nature and the environment. Most of the microorganisms carry out essential activities in nature, and many are closely associated with plants or animals in beneficial relations. These well-known microorganisms are the first example of the biotechnological process, concurring through the fermentation of some matrices, such as milk, meat, fish, grapevine, and cereals, in order to produce foods that are vital elements in the human diet. The use of these microorganisms is also essential for the production of new functional products or ingredients containing, for instance, immobilized probiotic/synbiotic formulae entrapped in safe matrices. Additionally, in this form, their vitality is preserved during some food technological processes or along the gastrointestinal tract.

Simultaneously, several bacteria are undesired or even pathogens, concurring in some cases to alter the quality and healthy characteristics of food, and in many instances to cause important diseases (human, animal or even vegetal). Generally, they are found in all of the environments, in the microbiota (both animal and vegetal) and the water polluted with fecal material. Microbial diseases constitute one of the primary causes of death in many developing countries of the world. These microorganisms are resistant to environmental conditions. In addition, most of the human population is entirely susceptible, and the diseases they cause are severe with a high fatality rate. A considerable amount of these lethal microorganisms could readily be grown and conserved for many years. Moreover, the number of pathogens with resistance to conventional drugs is increasing. Generally, bacteria are present in the planktonic form. However, as their number increases, the microbial cells begin to organize themselves into structured microbial communities, encased in an extracellular matrix known as biofilms, capable of colonizing every surface animal, vegetal or even mineral, sediments, soil, as well as all of the varieties of biomedical implants and transcutaneous devices [1,2]. The physiology of microorganisms when forming the biofilm is different compared to the planktonic one. In this “new” form, they tend to be more resistant to the treatment with antibiotics and other biocides, which are protected by the envelope formed by exopolysaccharides and proteins [3,4]. Therefore, the development and use of more sensitive methodologies, capable of quickly detecting and monitoring a microbial population present in a specific biological matrix, as well as performing to allow for the study of all its metabolic changes (e.g., in the case of the formation of biofilm) to occur, is an essential requirement for both health and the food industry. Traditionally, the bio-molecular methodologies can replace standard methods of essential microbiology. However, although these methods are certainly faster than the former, they require some preliminary steps (DNA extraction, gene amplification by PCR-RT, material analysis), which can still cause an undesired loss of time.

In the case of biofilms, conventional methods based on plating and microscopic counting are suitable for the study and detection of the number of bacteria adhering onto eukaryotic cells or inanimate surfaces.

In the literature, the best-known methods that study and evaluate the biofilm formation are based on microtiter plates, developed by Madilyn Fletcher [5], in which the measurement of the biomass attached quantifies the biofilm [6,7]. In the first developed procedure, bacterial cells are grown in a polystyrene microtiter plate [8].

The planktonic cells are washed away for different observation times before staining the biomass attached to the wells' surface to remove the non-adherent cells. The biofilm biomass can alternatively be quantified by detachment and subsequent plating. One major limitation of this technique is that the extracellular polymeric substances (EPS) can cover parts of the biomass derived from the settled cells on the bottom of the well. Therefore, this biomass could come from the biofilm-forming process, thus introducing a non-negligible error. The Calgary biofilm device (CBD) [9], based on the application of pegs that fit into the wells of the microtiter plate, could prevent the biofilm formation from the settled cells. This system produces 96 equivalent biofilms, for the assay of antibiotic sensitivity through the standard 96-well technology. In this way, the biofilm formed on the pegs arises from a sessile development rather than cell sedimentation [10–12].

Moreover, biofilm formation is primarily investigated by quantitative microbiology and scanning electron microscopy. Nevertheless, some issues remain as the recovery of bacterial cells, which takes place through sonication, usually retrieves only a part of them. Furthermore, the physiological properties of the detached population may not reflect the physiology of sessile cells since different microbial populations may present diverse adhesions and thus, various detachments of material [13,14].

Another technology that has been developed more recently consists of the so-called Biofilm Ring Test [15,16] (Saint-Beauzire, France), which uses the immobilization of magnetic beads by the biofilm matrix, while growing *in vitro* [17,18].

It is possible to evaluate the capacity for biofilm formation through indirect methods. When the cell-matrix is not strong enough to trap and hold the microspheres, for instance, to overcome the attractive forces exerted by external magnets, this gives rise to a weak biofilm. Conversely, a biofilm formed more rapidly will quickly and effectively block the microparticles [19]. The absence of biofilm led to the attraction of beads to the center of the bottom wells and to the formation of a central point. The presence of the biofilm formation gives rise to the immobilization of beads, and the stain disappears. However, this methodology has some limitations for extensive use in a clinical setting since it requires the additional step of treating the cells with magnetic beads, resulting in the introduction of other variables that may influence the repeatability of the tests [20].

To the best of our knowledge, these methods are laborious and require a large amount of time. In addition, the bacteria should be viable after the releasing process. Other methods, such as those based on microscopy or colorimetric approaches, are also applied after fixation and Gram staining, but they are laborious. Currently, crystal violet (CV) staining is the most widely used method for *in vitro* quantification of biofilm due to its relative simplicity and sensitivity [21]. However, it is limited by evident factors, not least in the time of the procedure (24–48 h of incubation), multiple processing steps, large standard deviations of the readouts, and weak flexibility, if we do not want use it for large-scale screening.

At the present time, two techniques, in particular, have gained the attention of scientists: The first is the so-called “biospeckle”, an optical method, which is an innovative tool for applications in food quality, food safety, and nutraceuticals. Through this technique, we can evaluate and monitor—very quickly—the presence of bacteria (or their proliferation) in a solid or liquid biological matrix. Furthermore, through the decorrelation of the biospeckle, we can quantify and optimize the storage time of the probiotic bacteria encapsulated in alginate and their survival rate in simulated gastro-intestinal conditions.

In the last decade, a new family of biological applications uses ferroelectric crystals [22], including the fungal growth stimulated by laser interference gratings [23], and the bacterial patterning in water-based media [24], to cite some examples. In particular, for the first time, Rega et al. demonstrated the possibility of using the pyroelectric effect in ferroelectric materials for cell patterning [25–29] and soft matter manipulation [30–32].

Moreover, the same authors proposed the pyroelectric effect as a successful method for what has been called the “biofilm electrostatic test” (BET) [27–29,33]. This method allows for the study and monitor of the formation of a microbial biofilm, as well as the more or less aptitude of certain microorganisms in order to form a biofilm when grown in particular conditions. Therefore, more detailed and faster knowledge of the formation and most of the events concurring to form a biofilm are essential to control, manipulate or even eradicate the biofilms, depending on the field and situation. In addition, the development of faster and more sensitive techniques for the detection and study of biofilm is crucial if we want to test synthetic drugs or natural compounds with antimicrobial activity [34].

2. Biospeckle Analysis

From a mathematical viewpoint, we could consider speckle a random walk phenomenon in the complex plane [35]. When coherent light probes the rough surfaces, speckles originate on the recording device. If the surface roughness is comparable to the probe wavelength, let us model the surface under the test as consisting of L independent scatters, i.e., L independent new point sources placed in different 3D coordinates. Light scattered from each point reaches the detector after propagating through the medium (e.g., air, PBS, water), experiencing a different optical path. Therefore, the detector receives the coherent superposition of the L complex wave front contributions in the form of an intensity pattern:

$$I = \left| \sum_{i=1}^L U_i \right|^2 = \left| \sum_{i=1}^L \rho_i e^{j\psi_i} \right|^2 = \left| \sum_{i=1}^L \rho_i e^{j \frac{2\pi}{\lambda} OPD_i} \right|^2, \quad (1)$$

where $U_i \in \mathbb{C}^2$ denotes each single scattering contribution; ρ_i and ψ_i represent the modulus and period of the i -th term; OPD_i represents the corresponding experienced optical path delay; and λ is the wavelength (the dependence on the spatial variables has been excluded in Equation (1) for the sake of conciseness). Figure 1 sketches the random walk process for the neighbor pixels of the detector, showing how much the OPD differences between each contribution govern this. Although similar gray levels could represent close-by points of a macroscopically homogeneous surface after detector quantization, the random walk process generates different results from the coherent sum. This situation is primarily due to the wavenumber factor ($2\pi/\lambda$) in the argument of U_i that amplifies any tiny OPD difference. Therefore, the pixels in Figure 1a are represented by different values, resulting in the typical sequence of bright and dark spots in a speckle representation.

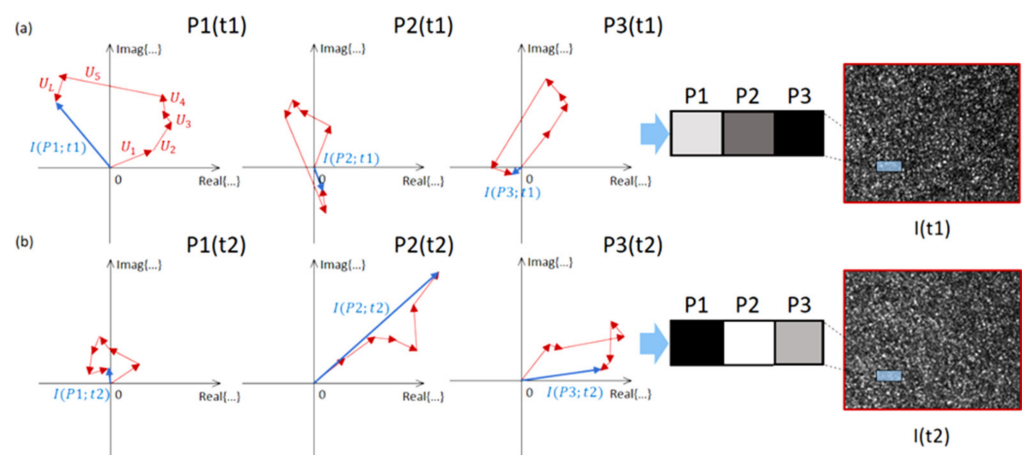


Figure 1. Random walk in the complex plane. The process of speckle grains formation at the receiver is sketched for three close-by pixels of a homogeneous region of the image. The resultant of each coherent sum is indicated with a blue arrow. (a) $t = t_1$. (b) $t = t_2$.

A speckle is thought of as an impairment for imaging, and many speckle reduction techniques have been proposed over the years. However, speckle grains represent a precious source of information, which is the coherent sum sensitive to sub-micrometric time variations of the rough surface, i.e., changes occurring on the scale of the probe wavelength. In microscopy configurations, it is helpful to study the formation of speckle patterns generated when light is reflected/refracted from a scattering medium to infer information on the medium itself. Furthermore, the size, spatial, and frequency distribution of the speckle grains can be linked to the shape of the scattering object, its roughness, as well as the superficial or volumetric density [35–38]. For these reasons, optical speckle metrology has become one of the most sensitive classes of measurement techniques, and it is adopted in many different industrial fields for non-destructive testing (NDT) of macroscopic size objects [39].

Among the wide variety of methods that use speckles to retrieve information on the presence of biological activity inside a specific field of view (FoV), we can distinguish between the static approaches, where speckles do not change over time, and the dynamics ones, influenced by the optical Doppler effect that leads to speckle changes over time. Therefore, the dynamic speckles contain information on the object's movement or the motion of particles within the object.

Regarding the possibility of studying the static scattering properties of a single biological element, a sizeable numerical aperture (NA) microscopy setup is mostly required, which sacrifices the available FoV [40–43]. However, measurements of light-scattering profiles with a scanning flow cytometer have morphologically differentiated T- and B-lymphocytes, providing the cell diameter, the ratio of nucleus to cell diameter, and the refractive index of the nucleus and cytoplasm for each cell [42]. Furthermore, the model-specific solution of the inverse light-scattering problem (ILS) [42] has been applied in the bacterial field. In

particular, ILS retrieves the length and diameter of single *Escherichia coli* bacteria relying on a hemisphere-capped cylinder model, shaping each element [40]. The rod-like shape allowed for the classification among four different bacteria species looking at the Fourier transform light scattering (FTLS) pattern [41]. Furthermore, a single *E. coli* cell diffraction pattern has been imaged at near-atomic resolution by coherent X-rays, simply by combining each particle diffraction by X-ray free-electron lasers [43].

Rather than looking at one single element, an ensemble characterization is required to acquire information from a large FoV in order to infer statistically relevant data. For example, in the case of bacteria, the way a cell affects light propagation has been intensely investigated [44–48].

The Fresnel diffraction pattern acquired through transmission can represent a fingerprint of specific species, i.e., the captured diffraction rings are unique markers enabling classification from heterogeneous samples [44,49]. Elastic light scattering (ELS) collects transmitted light from multiple angles to infer the size of bacteria populations (*Pseudomonas aeruginosa*, *Staphylococcus aureus*, and *Bacillus subtilis*) of various dimensions and shapes in the absence of prior information, providing a method to monitor the environment for microbial contamination [45].

A multispectral approach on ELS patterns from bacterial colonies has been performed [50], although it is feasible in the absence of sample movements, and capable of providing different spectral responses via wavelength-dependent refractive indices. Similarly, a fingerprint of specific colonies can be obtained using Fourier transform Raman spectroscopy, which is fast in gaining spectra and in non-disruptive modality [51].

Lens-less imaging has been involved in cell monitoring to achieve a large FoV, maintaining microscopic resolution, image quality, and easy implementation [52]. However, similar to bacteria, small objects might not diffract enough light to be detected depending on the culture medium of dipping. According to this purpose, a thin wetting film lens-less imaging has been developed for micro-objects detection and counting [53,54], such as bacteria, bragging about a considerable FoV by a compact system combined with in-line holographic reconstruction [53].

Accuracy and specificity in classifying various populations co-existing in the same heterogeneous sample can be largely improved by widening the observable space. An excellent example in this sense is the class of methods relying on hyperspectral imaging (HSI) [46]. HSI captures a wide range of wavelengths (from 200 nm to 2 μ m) to enlarge the observable space and has been successfully applied to the static inspection of the quality of meat, fruit, and seafood, by detecting defects, imperfections, assessing ripeness, and aging, as well as the presence of bacteria colonies [47,49,53]. These methods acquire spatial maps of the objects inside the FoV by tuning the wavelength of the light source from the ultraviolet to the NIR region and stacking the captures in the so-called hypercube. However, the large dimensionality of the hypercube makes it cumbersome to handle unless efficient data reduction is applicable (e.g., using the principal component analysis, PCA) [53]. Furthermore, the large extent of the information stored in the hypercube can be univocally associated with a specific population of biological elements. For example, the prediction of *E. coli* contamination has been determined thanks to the scattering information collected in HSI [47]. Similarly, a NIR hyperspectral imaging system (900–1700 nm wavelength range) has been employed to predict and visualize the total Enterobacteriaceae loads in the raw chicken breast fillets [54]. Moreover, NIR HSI is suitable for quantifying total viable counts in chicken breast fillets, leveraging the method's rapidness and non-destructiveness characteristics [55]. Therefore, the need for fast detection, classification, and discrimination systems for foodborne bacterial pathogens with high sensitivity and specificity is pivotal in food safety control, allowing for the HIS spread in food safety, which is deeply reviewed in [55]. Even a multimode approach has been presented to address food safety and quality importance, the joint action of spectroscopic methodologies involving hyperspectral reflectance, fluorescence mapping, Raman, and speckle imaging to improve detection performance [56].

Rather than investigating the static features of scattering patterns, the approaches based on the time variations of the biospeckles study the temporal decorrelation occurring as a consequence of biological activity inside the FoV [57–62]. In this type of analysis, we can consider $U_i = U_i(t)$ and, in turn, $I = I(x,y;t)$, where x and y are the spatial variables and t denotes the time variable. Any variation on the object surface occurring on the wavelength scale, although not visible by naked-eye inspection, determines a change in the coherent sum of Equation (1), in order for the intensity and positions of the speckles to vary and be detected. The success of this type of analysis is mainly due to the simplicity of the recording setup. It only requires shining coherent light onto the surface to investigate and record the scattered speckle pattern for a specific time window. In addition, a simple NA microscope objective with a small magnification allows us to capture images of the speckle pattern, which allows collecting speckle spots from a large FoV. Details on the setups usually applied in this case can be found in [63,64]. Biospeckle time monitoring has been applied in the field of food preservation to observe the action of endogenous enzymes responsible for the aging process occurring in beef [65], in biomedicine and neuroscience to image the retinal blood flow, as well as micro-flows in the skin and brain tissue [63], and to visualize perfusion in different tissues [65]. In particular, the laser speckle contrast imaging (LSCI) is a very suitable tool for the imaging of tissue perfusions since flowing red blood cells promote dynamic changes in the backscattered light. A very comprehensive review of LSCI can be found in [65].

Widening the observable space can improve the accuracy and specificity in classifying various populations co-existing in the same heterogeneous sample. An excellent example in this sense is the class of methods relying on hyperspectral imaging (HSI) [46]. HSI captures a wide range of wavelengths (from 200 nm to 2 μ m) to enlarge the observable space and has been successfully applied to the static inspection of the quality of meat, fruit, and seafood, by detecting defects, imperfections, assessing ripeness, and aging, as well as the presence of bacteria colonies [47,49,55]. These methods acquire spatial maps of the objects inside the FoV by tuning the wavelength of the light source from the ultraviolet to the NIR region and stack the captures in the so-called hypercube. However, the large dimensionality of the hypercube makes it cumbersome to handle unless efficient data reduction is applicable (e.g., using the principal component analysis, PCA) [55].

Moreover, the large extent of the information stored in the hypercube can be univocally associated with a specific population of biological elements. Prediction of *E. coli* contamination has been determined thanks to the scattering information collected in HSI [47]. Similarly, a NIR hyperspectral imaging system (900–1700 nm wavelength range) can predict and visualize the total Enterobacteriaceae loads in the distribution of raw chicken breast fillets [56]. Moreover, NIR HSI is suitable for quantifying total viable counts in chicken breast fillets, leveraging the method's rapidness and non-destructiveness characteristics [66]. Therefore, the need for fast detection, classification, and discrimination systems for foodborne bacterial pathogens with high sensitivity and specificity is pivotal in food safety control, allowing for the HSI spread in the food safety field, which is deeply reviewed in [67]. Even a multimode approach may address food safety and quality importance. In addition, the joint action of spectroscopic methodologies involving hyperspectral reflectance, fluorescence mapping, Raman, and speckle imaging improves detection performance [68].

Rather than investigating the static features of scattering patterns, the approaches based on the time variations of the biospeckle study the temporal decorrelation occurring as a consequence of biological activity inside the FoV [57–62]. In this type of analysis, we can consider $U_i = U_i(t)$, and, in turn, $I = I(x,y;t)$, where x and y are the spatial variables and t denotes the time variable. Any variation on the object surface occurring on the wavelength scale, although not visible by naked-eye inspection, determines a change in the coherent sum of Equation (1), in order for the intensity and positions of the speckles to vary and be detected. The success of this type of analysis is mainly due to the simplicity of the recording setup. It only requires shining coherent light onto the surface to

investigate and record the scattered speckle pattern for a specific time window. A simple NA microscope objective with a small magnification allows us to capture images of the speckle pattern, which allows collecting speckle spots from a large FoV. References [63,64] can provide details on the setups usually applied in this case. Biospeckle time monitoring has been used in the field of food preservation to observe the action of endogenous enzymes responsible for the aging process occurring in beef [59], in biomedicine and neuroscience to image the retinal blood flow, as well as microflows in the skin and brain tissue [60], and to visualize perfusion in different tissues [65]. In particular, the laser speckle contrast imaging (LSCI) is a very suitable tool for the imaging of tissue perfusions since flowing red blood cells promote dynamic changes in the backscattered light. By analyzing the temporal variations of speckle patterns, Yeo et al. observed that the addition of a disinfectant led to an inverse correlation between *E. coli* bioactivity and the contrast of speckle images, and the lower the bioactivity, the higher the contrast [69]. Another study on biodynamic speckle for *E. coli* bioactivity detection in suspension confirmed that the higher the disinfectant concentration, the lower the contrast in speckle images, indicating bacteria motility and viability reduction [70]. The dynamic speckle method combined with a temporal difference processing has fully characterized *E. coli* activity in Petri dishes, differentiating the inoculated compartment activity from the non-inoculated one during different stages of bacteria growth [71]. Nonetheless, the capability of biospeckle images in bacterial chemotactic response evaluation [72] and the activity profile of bacterial cultures differentiation have been assayed [73]. Compared to conventional techniques, the effectiveness of the dynamic laser speckle method has led to a quick and easy discrimination between the filamentous fungi and motile bacteria on agar plates [74]. The laser speckle contrast imaging technique in bacterial activity detection has reached 2–3 h, which is faster than the other standard counting methods [75]. The decrease of the speckle grain size when a medium scattering coefficient is enhanced has allowed for the assessment of two bacterial growth phases: One exponential highlighting bacteria increasing and one stationary indicating sporulation and cell lysis [76]. Moreover, the laser speckle contrast analysis (LASCA) is helpful in the genetic field, detecting the gene diversity by spatial LASCA processing [77,78].

Furthermore, time decorrelation due to bacteria activity has been studied to evaluate fruit quality during shelf-life [79], the conservation status of chicken and turkey breast tissues, detecting the presence of *E. coli* and *Bacillus cereus* [59,80], and distinguishing between fresh and contaminated water [59].

The previously implemented dynamic laser speckle (DLS) methods are optical lab-limited methods [81,82]. Nevertheless, an increasingly growing field has emerged, pushed by the need to bring speckle-imaging capabilities out of the lab. In reference [81], Braga et al. developed a portable device, smartphone-based, for DLS data acquisition and analysis, with the ability to set camera parameters and extract frames from recorded videos, pivotal for a portable solution [83].

In addition, the recent advances in machine learning have pushed the growth of AI-assisted biospeckle imaging. In this respect, the combination of various descriptors can classify different bioactivities occurring in non-neighboring portions of the specimen surface [84,85]. An excellent example in this sense is the possibility to digitally mark healthy and bruising regions in apples following this paradigm [84].

The case of self-propelling bacteria assumes particular importance since a bacterial colony decorrelates the speckles in time as a moving diffuser [64], i.e., bacteria move for distances larger than λ , thus changing the way the probe light sees the surface roughness. In turn, the succession of dark and bright spots in Figure 1b is different from the pattern corresponding to the same subset of pixels in Figure 1a. One can use these time changes to discover living microorganisms on the food surface or in a liquid environment, by measuring the correlation coefficient between the speckle patterns acquired at different times.

$$C(x, y; \tau) = \frac{1}{T - \tau} \sum_{t=1}^{T-\tau} I(x, y; t) I(x, y; t + \tau) \Delta t, \quad (2)$$

where τ represents the time lag, while Δt denotes the time resolution. The speckles are expected to keep static and C to approach the unity where the biological activity is lacking. A decrease of correlation over time indicates that microbial activity is taking place over the surface under test. Different correlation saturation values are expected for different densities of bacteria inside the FoV. Remarkably, during our experiments, we simulated out of the lab conditions in order for the vibration isolation system of the optical table that we used to be turned off. This choice allows us to check the approach's performance when the system is developed as a field-portable device, e.g., for use by food companies in the production lines or by customers at the points of sale in the next future.

As a consequence, C is not expected strictly equal to unity over time, and the slight decrease of correlation determines the limit of detection of our system. The biospeckle analysis revealed the presence of different concentrations of *B. cereus* on the surface of ham slices. The test clearly indicated the possibility of detecting *B. cereus* with concentrations ranging from 2×10^8 to 3×10^7 units/mL in less than 5 s [59]. Then, the same system was capable of assessing the microencapsulation performance of two probiotics, namely *Lactocaseibacillus rhamnosus* and *Lactiplantibacillus plantarum*, entrapped in capsules of alginate, during the treatment with different simulated gastrointestinal conditions [63]. The test evidenced that capsules protect bacteria during the passage through the acidic conditions present in the stomach and allow for the release of bacteria only when they reach the intestine (with a basic environment). We dipped capsules inside the three different liquids, namely PBS, acid, and basic solutions. We verified that speckles decorrelation could be observed only for alginate microcapsules floating inside the basic solution for both the probiotic species. As for the PBS and acid solution, speckle decorrelation is observed, but the correlation saturation value is comparable to the value obtained in the control experiment, i.e., it is likely due to external vibrations and floating of the capsules inside the liquid. By repeating the experiments at different concentrations of probiotics, we determined the limit of detection, which is $OD = 0.5$, i.e., 4×10^8 units/mL. The presence of a liquid environment worsens the detection limit in the case of microencapsulation assays due to capsules' unwanted floating. However, the reported value is small enough for this application to infer information on the microencapsulation performance. Over a number of weeks, we replicated the test and predicted the shelf time for microcapsules filled with the two probiotic species. Although the alginate material continued to encapsulate both species effectively, *L. rhamnosus* demonstrated higher shelf-time (9 weeks against the 3–4 weeks of the *L. plantarum*) [63].

In addition to studying the temporal correlation coefficient between the speckle patterns, an alternative approach to visually assess the time variability of the speckles, the time history speckle pattern (THSP) matrix, and the co-occurrence matrix (COM) can be calculated [48,86]. The former is built by sampling the 3D stack $I(x, y, t)$ as:

$$THSP_0 = I(x, y, t)|_{y=y_0} = I(x, y_0, t), \quad (3)$$

where y_0 is the sampled column [48]. In the case of static speckles, $THSP_0$ appears as a replica along one direction of the column y_0 . In the case of a biospeckle activity, $THSP_0$ shows a speckle-like pattern in the (x, t) domain. The COM of the THSP is defined as [86]:

$$COM = \left[\frac{N_{jk}}{\sum_k N_{jk}} \right], \quad (4)$$

where j and k span across the entire dynamic range, and N_{jk} is the number of times the intensity level k occurs right after the level j . By definition, in the case of static speckles and no intensity fluctuations, the COM is the identity matrix, while a spread of values different from zero can be seen around the main diagonal in the case of biospeckle activity. In addition to the qualitative information obtained by visual inspection of the COM, some

metrics are usually defined to quantify the spread around the diagonal. For example, the inertia moment (IM) is a second-order moment defined as:

$$IM = \sum_{j,k} \left\{ \frac{N_{jk}}{\sum_k N_{jk}} (j - k)^2 \right\}, \tag{5}$$

and provides an objective, quantitative measure of speckle temporal changes due to bioactivity [48,86]. Although not recent, monitoring the biological activity by dynamic biospeckle is a still-growing field broadly discussed and intensely employed in many areas of knowledge [83].

3. Biofilm Electrostatic Test

The formation of bacterial biofilm and adhesive processes to several surfaces by bacteria and fungi has substantial implications in food manufacturing, as well as transformation and health-linked areas. The cellular mechanisms that regulate the formation of bacterial biofilm are still under study. In addition, their control is an objective for new specific interventions and plans to manage the problems due to the biofilm formation and presence. In particular, the food decline does not only translate into economic losses. Food safety is one of the main priorities in today's globalized market. The interaction between three main components, bacterial cells, growth medium, and the environment surrounding the bacterial attachment surface, affects the adhesion of the bacterial cells and the subsequent biofilm. Managing the interactions between bacteria and surface allows us to have a powerful tool capable of controlling the formation of bacterial biofilm.

We recently proposed the innovative BET technique to promote rapid biofilm formation through the electrostatic interaction with charged polymer sheets. The technique induces a permanent dipole charge into thin polymer sheets by pyro-electrification (PE) [25–29]. The technique appears to be versatile, reproducible, simple, and easy to use for multipurpose applications, ranging from live-cell patterning to bacteria biofilm formation tests [25–29]. Figure 2 shows the schematic view of the PE process.

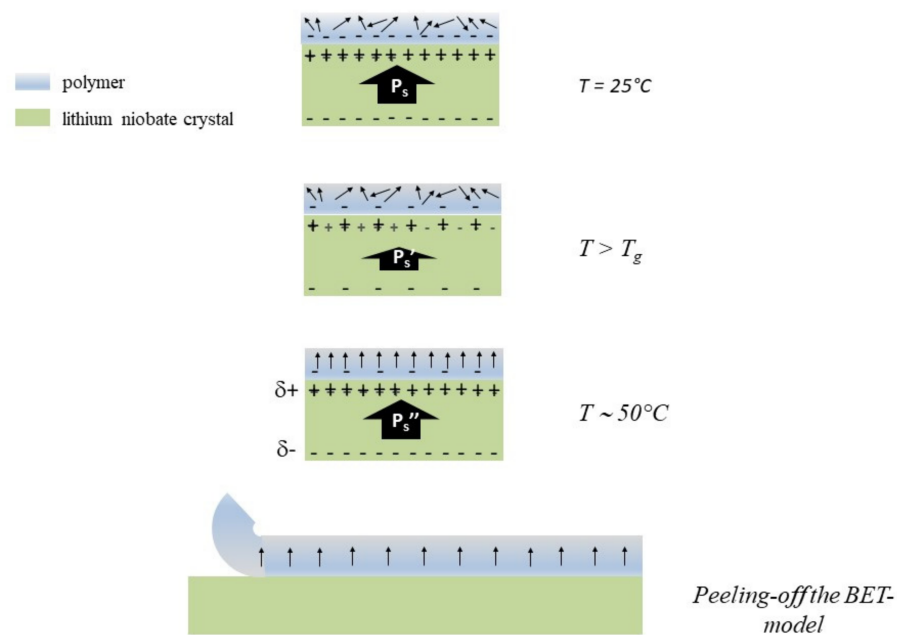


Figure 2. Schematic representation of the PE process steps with the corresponding charge distributions.

The process consists of slowly heating a polymer film spin-coated on a substrate of lithium niobate crystal (LN) to a temperature higher than the glass transition temperature (T_g) of the polymer. Next, the treatment of the substrate (with the film deposited on

its surface) to different temperatures induces a fast temperature gradient and creates a pyro-electric macroscopic field. At this condition, the polymer molecules can reorient under the effect of the uncompensated surface pyro-electric charge of LN and, when the intermolecular motion stops, the molecules “freeze” in a poled configuration. After that, the polymer film can be peeled off from the LN substrate, producing free-standing polarized membranes. Regarding the conventional electrification techniques, the PE is electrode-free, thus simplifying the process significantly. See Ref. [25] for more details.

The assessment of microbial capability to adhere to and form biofilms is essential for evaluating how different environmental factors may affect their vitality. Currently, the approaches used are still weak in reliability and rapidity and frequently give conflicting results. BET appears to be an easy, fast, and highly replicable instrument for estimating the in vitro capacity of bacteria in order to form biofilms through an electrostatic interaction with a pyro-electric carrier.

The rapid bacterial adhesion and formation of biofilms endorsed by BET would substantially affect health assistance, when a quick answer to an antibiogram test would allow for an immediate cure to fight those diseases giving rise to bacterial infections.

BET sheets stimulate rapid adhesion and biofilm formation by *Listeria innocua* (Gram-positive) and *E. coli* (Gram-negative) bacteria strain. The method admits an easy, fast, and economically efficient evaluation of biofilm formation, using the electrostatic interaction between the planktonic bacteria with the pyro-electric support [27,29].

After the pyro-electrification process, the BET-carrier is provided by the $\delta +$ charge of the permanent dipole, which is capable of immobilizing the bacteria without any damage to their cytomembrane. The negative net charge present on the bacterial cytomembrane (COO-groups) of both Gram-positive and Gram-negative bacteria is attracted by positive polarity on each surface, shown in Figure 3, conducting bacteria adhesion and immobilization and biofilm formation [87]. Therefore, the bacterial adhesion and consequent biofilm formation are faster on the BET support since the positive polarization charge on the BET support increases the Coulomb interaction strength, in agreement with the DLVO theory, according to which [88] bacteria adhere to the surface when they manage to overcome the minimum secondary energy.

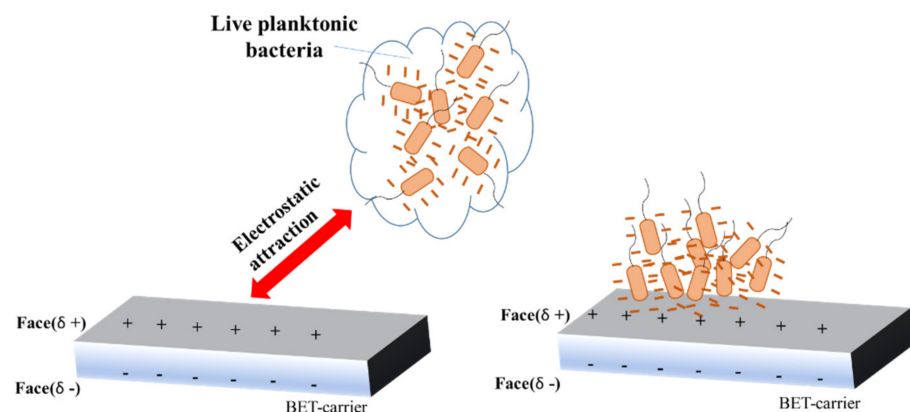


Figure 3. Schematic point of view of the bacterial cells interaction model with the BET-carrier. Face ($\delta+$) and Face ($\delta-$) indicate the polarity of the BET-carrier faces.

The images represented in Figure 4 show that the tested BET provides a polarization field capable of immobilizing *L. innocua* (Figure 4a) and *E. coli* (Figure 4b) by promoting the formation of live biofilms already within 2 h, avoiding strenuous incubations and intermediary chemical treatments. Figure 4 shows the production of two types of Polysulfone BET sheets (thickness of about 100 μm and dimensions $2 \times 2 \text{ cm}^2$): Bare sheet (not subjected to the pyro-electrification process) representing the control; and (BET) with the positive side in contact with the bacterial suspension. The incubation of the sheet at 37 $^{\circ}\text{C}$, at two times (2 and 4 h) and in two different Petri dishes overlaid with 500 μL of bacterial suspension, is

then followed by the observation at the optical microscope and by the comparison with the control.

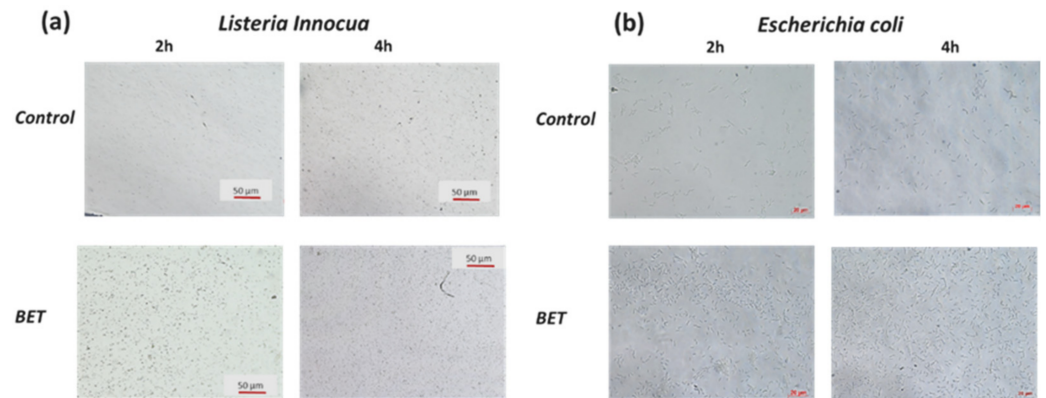


Figure 4. (a) Optical microscopy images of bacterial adhesion of *L. innocua* at two different time points on the control and BET; (b) optical microscopy images of bacterial adhesion of *E. coli* at two different time points on the control and BET.

The amount of adherent bacteria on the BET, consequent to the biofilm form, in both bacterial strains was visibly higher than the control at each observation time.

BET allows us to have the scenario of a 24-h biofilm of both Gram-negative and Gram-positive bacteria within 2 h and with 6-fold higher density than the control. Due to the structural integrity of the cell membrane, the BET-carrier is capable of supporting the growth of a vital biofilm even after 24 h incubation and with a growth rate 6-fold higher than the control. The live/dead staining kit admits to monitoring biofilms' viability (see Figure 5). After 24 h of incubation, we can see that the viability of the high-density biofilms formed on the BET sheet is evident in Figure 5. The BET sheet immobilizes the planktonic bacteria more quickly than the control, favoring the biofilm formation without damaging the bacterial cell membrane even after 24 h of incubation, thus proving their biocompatibility. Conversely, chemical coatings that usually immobilize planktonic bacteria could damage their cell membrane, causing death.

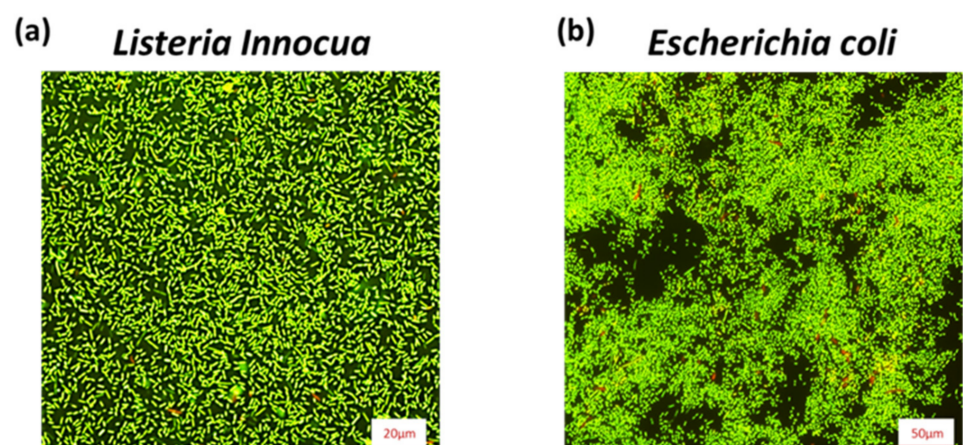


Figure 5. Fluorescence microscope images of *L. innocua* (a) and *E. coli* (b) forming a biofilm on the BET sheet after 24 h incubation and live/dead staining.

Further quantitative studies evaluated the practical efficiency of the BET vector. In particular, the biomass quantity adhered on the BET vector surface was determined in the early stages of bacteria incubation. In this analysis, two bacterial suspensions of *E. coli* were used with two different concentrations differing by approximately one order of magnitude in terms of optical density (OD), and the biomass amount was assessed through the CV

assay [89]. Figure 6 shows the typical optical microscope images after CV staining. The results obtained in the first 2 h demonstrate the ability of the BET vector to promote faster biofilm formation than the control surface, even in the case of highly diluted bacterial concentration [29].

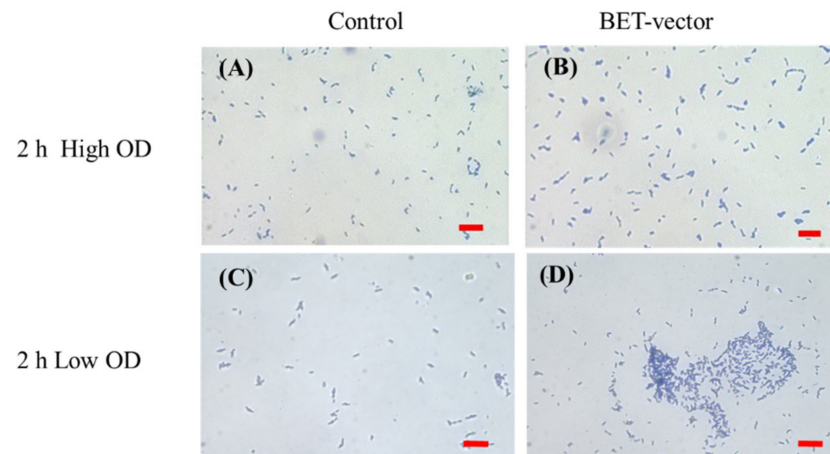


Figure 6. Crystal violet microscope images of *E. coli* forming a biofilm on the BET sheet vs. control after 2 h of incubation for different OD initial values. (A,B) represent the images of High-OD *E. coli* forming a biofilm in the control and on the BET sheet, respectively, after 2 h of incubation. (C,D) represent the images of Low-OD *E. coli* forming a biofilm in the control and on the BET sheet, respectively, always after 2 h of incubation.

Figure 7a,b plots the data corresponding to the biomass determination for two different OD values. Either in high OD or low OD cases, the BET-carrier effectiveness (orange columns) has been demonstrated to immobilize a greater biomass quantity for each observation time than the control, with an increase of about 30% after 2 h for both cases. Moreover, the major amount of biomass on the BET-carrier was observed for 4-h incubation times, by 60% and 40%, respectively.

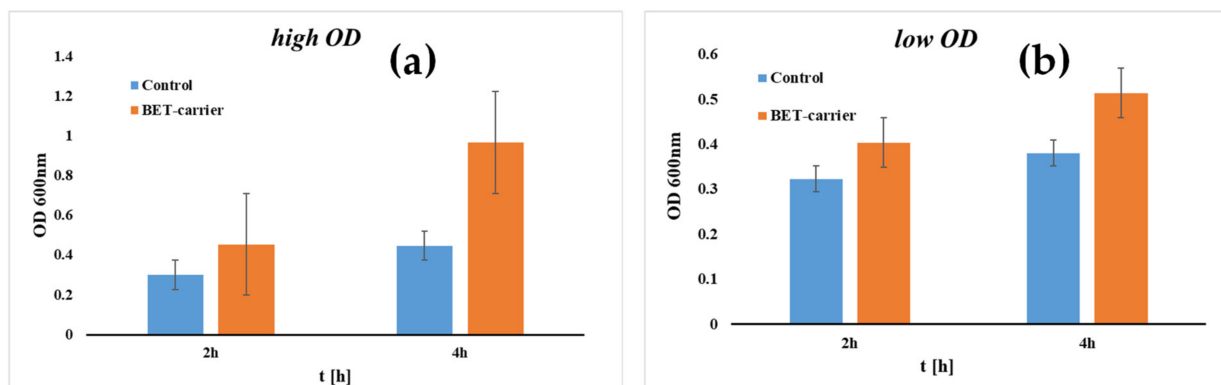


Figure 7. Quantitative determination of the biofilm adhered on the sheets by the CV absorbance in the case of the control (blue columns) and BET-carrier (orange columns) at the two incubation times, in the case of high OD (a) and low OD (b). The error bars represent the standard deviation for the three replicates of the experiment.

The BET-carrier ability to produce biofilms with high biomass in a few hours, even at low bacterial concentrations, is evident, with a significant impact [29].

4. Conclusions

We believe that these two techniques would be promising tools for both monitoring the growth of bacteria very quickly, and evaluating, just as speedily, the capacity of bacteria to form a biofilm, even in the presence of a minimal amount of bacteria. Therefore, these techniques would considerably affect the early detection of bacteria in several kinds of matrices, for food purposes and in the health field, allowing for a fast determination of the antimicrobial susceptibility.

Author Contributions: Conceptualization, S.G., E.O., M.M., R.R., B.M., V.B., F.N. and P.F.; methodology and investigation, S.G., E.O., M.M., R.R., B.M., V.B., F.N. and P.F.; writing—original draft preparation, S.G., E.O., M.M., R.R., B.M., V.B., F.N., M.V., R.C. and P.F.; supervision, S.G. and P.F. All authors have read and agreed to the published version of the manuscript.

Funding: The authors acknowledge the EU funding within the Horizon 2020 Program, under the FET-OPEN Project SensApp, grant agreement no. 829104 and project “PON Dottorati industriali” DOT1649008.

Institutional Review Board Statement: Not applicable.

Informed Consent Statement: Not applicable.

Data Availability Statement: Not applicable.

Conflicts of Interest: The authors declare no conflict of interest.

References

1. Bos, R.; van der Mei, H.C.; Busscher, H.J. Physico-Chemistry of Initial Microbial Adhesive Interactions—its Mechanisms and Methods for Study. *FEMS Microbiol. Rev.* **1999**, *23*, 179–230. [[CrossRef](#)]
2. Hall-Stoodley, L.; Costerton, J.W.; Stoodley, P. Bacterial Biofilms: From the Natural Environment to Infectious Diseases. *Nat. Rev. Microbiol.* **2004**, *2*, 95–108. [[CrossRef](#)]
3. Conlon, B.P.; Nakayasu, E.S.; Fleck, L.E.; La Fleur, M.D.; Isabella, V.M.; Coleman, K.; Leonard, S.N.; Adkins, J.N.; Lewis, K. Activated ClpP Kills Persisters and Eradicates a Chronic Biofilm Infection. *Nature* **2013**, *503*, 365–370. [[CrossRef](#)]
4. Hook, A.L.; Chang, C.Y.; Yang, J.; Luckett, J.; Cockayne, A.; Atkinson, S.; Mei, Y.; Roger Bayston, R.; Irvine, D.J.; Langer, R.; et al. Combinatorial Discovery of Polymers Resistant to Bacterial Attachment. *Nat. Biotechnol.* **2012**, *30*, 868–875. [[CrossRef](#)]
5. Fletcher, M. The effects of culture concentration and age, time, and temperature on bacterial attachment to polystyrene. *Can. J. Microbiol.* **1977**, *23*, 1–6. [[CrossRef](#)]
6. Ferreira, V.; Wiedmann, M.; Teixeira, P.; Stasiewicz, M.J. *Listeria monocytogenes* persistence in food-associated environments: Epidemiology, strain characteristics, and implications for public health. *J. Food Prot.* **2014**, *77*, 150–170. [[CrossRef](#)]
7. Borucki, M.K.; Peppin, J.D.; White, D.; Loge, F.; Call, D.R. Variation in biofilm formation among strains of *Listeria monocytogenes*. *Appl. Environ. Microbiol.* **2003**, *69*, 7336–7342. [[CrossRef](#)]
8. Djordjevic, D.; Wiedmann, M.; McLandsborough, L.A. Microtiter plate assay for assessment of *Listeria monocytogenes* biofilm formation. *Appl. Environ. Microbiol.* **2002**, *68*, 2950–2958. [[CrossRef](#)]
9. Ceri, H.; Olson, M.E.; Stremick, C.; Read, R.R.; Morck, D.; Buret, A. The Calgary Biofilm Device: New technology for rapid determination of antibiotic susceptibilities of bacterial biofilms. *J. Clin. Microbiol.* **1999**, *37*, 1771–1776. [[CrossRef](#)]
10. Harrison, J.J.; Ceri, H.; Yerly, J.; Stremick, C.A.; Hu, Y.; Martinuzzi, R.; Turner, R.J. The use of microscopy and three-dimensional visualization to evaluate the structure of microbial biofilms cultivated in the Calgary Biofilm Device. *Biol. Proced. Online* **2006**, *8*, 194–215. [[CrossRef](#)]
11. Ali, L.; Khambaty, F.; Diachenko, G. Investigating the suitability of the Calgary Biofilm Device for assessing the antimicrobial efficacy of new agents. *Bioresour. Technol.* **2006**, *97*, 1887–1893. [[CrossRef](#)]
12. Edmonds, J.M.; Collett, P.J.; Valdes, E.R.; Skowronski, E.W.; Pellar, G.J.; Emanuel, P.A. Surface sampling of spores in dry-deposition aerosols. *Appl. Environ. Microbiol.* **2009**, *75*, 39–44. [[CrossRef](#)]
13. Grand, I.; Bellon-Fontaine, M.N.; Herry, J.M.; Hilaire, D.; Moriconi, F.X.; Naitali, M. Possible overestimation of surface disinfection efficiency by assessment methods based on liquid sampling procedures as demonstrated by in situ quantification of spore viability. *Appl. Environ. Microbiol.* **2011**, *77*, 6208–6214. [[CrossRef](#)] [[PubMed](#)]
14. Azeredo, J.; Azevedo, N.F.; Briandet, R.; Cerca, N.; Coenye, T.; Costa, A.R.; Desvaux, M.; Di Bonaventura, M.; Hébraud, M.; Jaglic, Z. Critical review on biofilm methods. *Cri. Rev. Microbiol.* **2017**, *43*, 313–351. [[CrossRef](#)] [[PubMed](#)]
15. Olivares, E.; Badel-Berchoux, S.; Provot, C.; Jaulhac, B.; Prévost, G.; Bernardi, T.; Jehl, F. The BioFilm Ring Test: A rapid method for routine analysis of *Pseudomonas aeruginosa* biofilm formation kinetics. *J. Clin. Microbiol.* **2016**, *54*, 657–661. [[CrossRef](#)] [[PubMed](#)]
16. Chavant, P.; Gaillard-Martinie, B.; Talon, R.; Hébraud, M.; Bernardi, T. A new device for rapid evaluation of biofilm formation potential by bacteria. *J. Microbiol. Methods* **2007**, *68*, 605–612. [[CrossRef](#)]
17. Nagant, C.; Tré-Hardy, M.; Devleeschouwer, M.; Dehaye, J.P. Study of the initial phase of biofilm formation using a biofomic approach. *J. Microbiol. Methods* **2010**, *82*, 243–248. [[CrossRef](#)]

18. Di Domenico, E.G.; Toma, L.; Provot, C.; Ascenzioni, F.; Sperduti, I.; Prignano, G.; Ensoli, F. Development of an in vitro assay, based on the biofilm ring test[®], for rapid profiling of biofilm-growing bacteria. *Front. Microbiol.* **2016**, *7*, 1429. [[CrossRef](#)]
19. Di Domenico, E.G.; Cavallo, I.; Guembe, M.; Prignano, G.; Gallo, M.T.; Bordignon, V.; Ensoli, F. The clinical Biofilm Ring Test: A promising tool for the clinical assessment of biofilm-producing *Candida* species. *FEMS Yeast Res.* **2018**, *18*, foy025. [[CrossRef](#)]
20. Crémet, L.; Corvec, S.; Batard, E.; Auger, M.; Lopez, I.; Pagniez, F.; Caroff, N. Comparison of three methods to study biofilm formation by clinical strains of *Escherichia coli*. *Diagn. Microbiol. Infect. Dis.* **2013**, *75*, 252–255. [[CrossRef](#)]
21. Stepanovic, S.; Vukovic, D.; Dakic, I.; Savic, B.; Svabic-Vlahovic, M. A Modified Microtiter-Plate Test for Quantification of Staphylococcal Biofilm Formation. *J. Microbiol. Methods* **2000**, *40*, 175–179. [[CrossRef](#)]
22. Blázquez-Castro, A.; García-Cabañes, A.; Carrascosa, M. Biological applications of ferroelectric materials. *Appl. Phys. Rev.* **2018**, *5*, 041101. [[CrossRef](#)]
23. Kukhtarev, N.V.; Kukhtareva, T.V.; Jones, J.; Ward, E.W.; Sarkisov, S.S.; Curley, M.J.; Sugak, D.Y. Interaction of micro-organisms (fungi and bacteria) with optical and electronic materials. In *Optical System Contamination: Effects, Measurements, and Control VII*; International Society for Optics and Photonics: Seattle, WA, USA, 2002; Volume 4774, pp. 272–279.
24. Miccio, L.; Marchesano, V.; Mugnano, M.; Grilli, S.; Ferraro, P. Light induced DEP for immobilizing and orienting *Escherichia coli* bacteria. *Opt. Lasers Eng.* **2016**, *76*, 34–39. [[CrossRef](#)]
25. Rega, R.; Gennari, O.; Mecozzi, L.; Grilli, S.; Pagliarulo, V.; Ferraro, P. Bipolar patterning of polymer membranes by pyroelectrification. *Adv. Mater.* **2016**, *28*, 454–459. [[CrossRef](#)]
26. Rega, R.; Gennari, O.; Mecozzi, L.; Grilli, S.; Pagliarulo, V.; Ferraro, P. Pyro-electrification of polymer membranes for cell patterning. In *AIP Conference Proceedings*; D'Amore, A., Acierno, D., Grassia, L., Eds.; AIP Publishing: Melville, NY, USA, 2016; Volume 1736, p. 020042. ISBN 978-0-7354-1390-0/. [[CrossRef](#)]
27. Gennari, O.; Marchesano, V.; Rega, R.; Mecozzi, L.; Nazzaro, F.; Fratianni, F.; Coppola, R.; Masucci, L.; Mazzon, E.; Bramanti, A.; et al. Pyroelectric Effect Enables Simple and Rapid Evaluation of Biofilm Formation. *ACS Appl. Mater. Interfaces* **2018**, *10*, 15467–15476. [[CrossRef](#)]
28. Rega, R.; Gennari, O.; Mecozzi, L.; Pagliarulo, V.; Mugnano, M.; Oleandro, E.; Nazzaro, F.; Ferraro, P.; Grilli, S. Pyro-electrification of freestanding polymer sheets: A new tool for cation-free manipulation of cell adhesion in vitro. *Front. Chem.* **2019**, *7*, 429. [[CrossRef](#)]
29. Oleandro, E.; Rega, R.; Mugnano, M.; Nazzaro, F.; Ferraro, P.; Grilli, S. Quantitative determination of rapid biomass formation on pyro-electrified polymer sheets. *Biofilm* **2021**, *3*, 100040. [[CrossRef](#)]
30. Gennari, O.; Rega, R.; Mugnano, M.; Oleandro, E.; Mecozzi, L.; Pagliarulo, V.; Grilli, S. A skin-over-liquid platform with compliant microbumps actuated by pyro-EHD pressure. *NPG Asia Mater.* **2019**, *11*, 1. [[CrossRef](#)]
31. Bhowmick, S.; Iodice, M.; Giofrè, M.; Breglio, G.; Irace, A.; Riccio, M.; Coppola, S. Investigation of pyroelectric fields generated by lithium niobate crystals through integrated microheaters. *Sens. Actuators A Phys.* **2017**, *261*, 140–150. [[CrossRef](#)]
32. Rega, R.; Gennari, O.; Mecozzi, L.; Pagliarulo, V.; Bramanti, A.; Ferraro, P.; Grilli, S. Maskless arrayed nanofiber mats by bipolar pyroelectrospinning. *ACS Appl. Mater. Interfaces* **2019**, *11*, 3382–3387. [[CrossRef](#)]
33. Lettieri, S.; Rega, R.; Pallotti, D.K.; Gennari, O.; Mecozzi, L.; Maddalena, P.; Ferraro, P.; Grilli, S. Direct Evidence of Polar Ordering and Investigation on Cytophilic Properties of Pyroelectrified Polymer Films by Optical Second Harmonic Generation Analysis. *Macromolecules* **2017**, *50*, 7666–7671. [[CrossRef](#)]
34. Nazzaro, F.; Fratianni, F.; De Martino, L.; Coppola, R.; De Feo, V. Effect of essential oils on pathogenic bacteria. *Pharmaceuticals* **2013**, *6*, 1451–1474. [[CrossRef](#)]
35. Goodman, J.W. Some fundamental properties of speckle. *J. Opt. Soc. Am.* **1976**, *66*, 1145. [[CrossRef](#)]
36. Bianco, V.; Memmolo, P.; Leo, M.; Montesor, S.; Distante, C.; Paturzo, M.; Pixart, P.; Javidi, B.; Ferraro, P. Strategies for reducing speckle noise in digital holography. *Light Sci. Appl.* **2018**, *7*, 48. [[CrossRef](#)]
37. Bianco, V.; Memmolo, P.; Paturzo, M.; Ferraro, P. On speckle suppression in IR digital holography. *Opt. Lett.* **2016**, *41*, 5226–5229. [[CrossRef](#)] [[PubMed](#)]
38. Montrésor, S.; Memmolo, P.; Bianco, V.; Ferraro, P.; Picart, P. Comparative study of multi-look processing for phase map de-noising in digital Fresnel holographic interferometry. *JOSA A* **2019**, *36*, A59–A66. [[CrossRef](#)] [[PubMed](#)]
39. Kreis, T. *Handbook of Holographic Interferometry: Optical and Digital Methods*; Wiley-VCH: Weinheim, Germany, 2005. [[CrossRef](#)]
40. Konokhova, A.I.; Gelash, A.A.; Yurkin, M.A.; Chernyshev, A.V.; Maltsev, V.P. High-Precision Characterization of Individual *E. coli* Cell Morphology by Scanning Flow Cytometry. *Cytometry A* **2013**, *83*, 568–575. [[CrossRef](#)]
41. Jo, Y.; Jung, J.; Kim, M.; Park, H.; Kang, S.; Park, Y. Label-free identification of individual bacteria using Fourier transform light scattering. *Opt. Express* **2015**, *23*, 15792–15805. [[CrossRef](#)]
42. Strokotov, D.I.; Yurkin, M.A.; Gilev, K.V.; Van Bockstaele, D.R.; Hoekstra, A.G.; Rubtsov, N.; Maltsev, V.P. Is there a difference between T- and B-lymphocyte morphology? *J. Biomed. Opt.* **2009**, *14*, 064036. [[CrossRef](#)]
43. Miao, I.; Hodgson, K.O.; Ishikawa, T.; Larabell, C.A.; LeGros, M.A.; Nishino, Y. Imaging whole *Escherichia coli* bacteria by using single-particle x-ray diffraction. *Proc. Natl. Acad. Sci. USA* **2003**, *100*, 110–112. [[CrossRef](#)]
44. Suchwalko, A.; Buzalewicz, I.; Podbielska, H. Computer-based classification of bacteria species by analysis of their colonies Fresnel diffraction patterns. In *Frontiers in Biological Detection: From Nanosensors to Systems*; International Society for Optics and Photonics: Seattle, WA, USA, 2012; Volume IV, p. 8212.

45. Katz, A.; Alimova, A.; Xu, M.; Rudolph, E.; Shah, M.K.; Savage, H.E.; Rosen, R.B.; McCormick, S.A.; Alfano, R.R. Bacteria size determination by elastic light scattering. *IEEE J. Sel. Top. Quantum Electron.* **2003**, *9*, 277–287. [[CrossRef](#)]
46. Qin, J.; Chao, K.; Kim, M.S.; Lu, R.; Burks, T.F. Hyperspectral and multispectral imaging for evaluating food safety and quality. *J. Food Eng.* **2013**, *118*, 157–171. [[CrossRef](#)]
47. Tao, F.; Peng, Y.; Li, Y.; Chao, K.; Dhakal, S. Simultaneous determination of tenderness and Escherichia coli contamination of pork using hyperspectral scattering technique. *Meat Sci.* **2012**, *90*, 851–857. [[CrossRef](#)]
48. Zdunek, A.; Adamiak, A.; Pieczywek, P.M.; Kurenda, A. The biospeckle method for the investigation of agricultural crops: A review. *Opt. Lasers Eng.* **2014**, *52*, 276–285. [[CrossRef](#)]
49. Ponder, E. Diffraction patterns produced by bacteria. *Exp. Biol.* **1934**, *11*, 54–57. [[CrossRef](#)]
50. Kim, H.; Doh, I.J.; Bhunia, A.K.; King, G.B.; Bae, E. Scalar diffraction modeling of multispectral forward scatter patterns from bacterial colonies. *Opt. Express* **2015**, *23*, 8545–8554. [[CrossRef](#)]
51. Yang, H.; Irudayaraj, J. Rapid detection of foodborne microorganisms on food surface using Fourier transform Raman spectroscopy. *J. Mol. Struct.* **2003**, *646*, 35–43. [[CrossRef](#)]
52. Isikman, S.O.; Sencan, I.; Mudanyali, O.; Bishara, W.; Oztoprak, C.; Ozcan, A. Color and monochrome lensless on-chip imaging of Caenorhabditis elegans over a wide field-of-view. *Lab Chip* **2010**, *10*, 1109–1112. [[CrossRef](#)]
53. Poher, V.; Allier, C.P.; Coutard, J.G.; Hervé, L.; Dinten, J.M. Lensfree in-line holographic detection of bacteria. *SPIE-OSA Biomed. Opt.* **2011**, *8086*, 808619.
54. Allier, C.P.; Hiernard, G.; Poher, V.; Dinten, J.M. Bacteria detection with thin wetting film lensless imaging. *Biomed. Opt. Express* **2010**, *1*, 762–770. [[CrossRef](#)]
55. Liu, L.; Ngadi, M.O. Hyperspectral Imaging for Food Quality and Safety Control. *Ethiop. J. Appl. Sci. Technol.* **2013**, *S11*, 51–59.
56. Yao-Ze, F.; El Masry, G.; Sun, D.W.; Scannell, A.G.M.; Walsh, D.; Morcy, N. Near-infrared hyperspectral imaging and partial least squares regression for rapid and reagentless determination of Enterobacteriaceae on chicken fillets. *Food Chem.* **2013**, *138*, 1829–1836.
57. Boas, D.A.; Dunn, A.K. Laser speckle contrast imaging in biomedical optics. *J. Biomed. Opt.* **2010**, *15*, 011109. [[CrossRef](#)]
58. Celena, I.; Roberto, A.; Braga, A., Jr.; Ramos, E.M.; Ramos, A.L.S.; Roxael, E.A.R. Application of biospeckle laser technique for determining biological phenomena related to beef aging. *J. Food Eng.* **2013**, *119*, 135–139.
59. Bianco, V.; Mandracchia, B.; Nazzaro, F.; Marchesano, V.; Gennari, O.; Paturzo, M.; Grilli, S.; Ferraro, P. Food quality inspection by speckle decorrelation properties of bacteria colonies. Optical Methods for Inspection, Characterization, and Imaging of Biomaterials III. *Proc. SPIE* **2017**, *10333*, 103331N. [[CrossRef](#)]
60. Ansari, M.Z.; Ramírez-Miquet, E.E.; Otero, I.; Rodríguez, D.; Darias, J.G. Real time and online dynamic speckle assessment of growing bacteria using the method of motion history image. *J. Biomed. Opt.* **2016**, *21*, 066006. [[CrossRef](#)] [[PubMed](#)]
61. Pajuelo, M.; Baldwin, G.; Rabal, H.; Cap, N.; Arizaga, R.; Trivi, M. Bio-speckle assessment of bruising in fruits. *Opt. Lasers Eng.* **2003**, *40*, 13–24. [[CrossRef](#)]
62. Ramírez-Miquet, E.E.; Darias, J.G.; Otero, I.; Rodríguez, D.; Murialdo, S.; Rabal, H.; Trivi, M. Biospeckle Technique for Monitoring Bacterial Colony Growth with Minimal Photo-Exposure Time Associated. *IFMBE Proc.* **2015**, *49*, 313–316.
63. Mandracchia, B.; Palpacuer, J.; Nazzaro, F.; Bianco, V.; Rega, R.; Ferraro, P.; Grilli, S. Biospeckle decorrelation quantifies the performance of alginate-encapsulated probiotic bacteria. *IEEE J. Sel. Top. Quantum Electron.* **2019**, *25*, 7200206. [[CrossRef](#)]
64. Bianco, V.; Marchesano, V.; Finizio, A.; Paturzo, M.; Ferraro, P. Self-propelling bacteria mimic coherent light decorrelation. *Opt. Express* **2015**, *23*, 9388–9396. [[CrossRef](#)]
65. Heeman, W.; Steenbergen, W.; Gooitzen, M.; van Dam, E.; Boerma, C. Clinical applications of laser speckle contrast imaging: A review. *J. Biomed. Opt.* **2019**, *24*, 080901. [[CrossRef](#)]
66. Yao-Ze, F.; Sun, D.W. Determination of total viable count (TVC) in chicken breast fillets by near-infrared hyperspectral imaging and spectroscopic transforms. *Talanta* **2013**, *105*, 244–249.
67. Bonah, E.; Huang, X.; Aheto, J.H.; Osae, R. Application of Hyperspectral Imaging as a Nondestructive Technique for Foodborne Pathogen Detection and Characterization. *Foodborne Pathog. Dis.* **2019**, *16*, 712–722. [[CrossRef](#)]
68. Vasefi, F.; Booth, N.; Hazifi, H.; Farkas, D.L. Multimode Hyperspectral Imaging for Food Quality and Safety. In *Hyperspectral Imaging in Agriculture, Food and Environment*; Maldonado, A.I.L., Rodriguez-Fuentes, H., Vidales Contreras, J.A., Eds.; IntechOpen Ltd.: London, UK, 2018; pp. 11–27. ISBN 978-1-78923-290-5. [[CrossRef](#)]
69. Yeo, B.A.; Watson, I.A.; Wong, J.W.M.; Stewart-Tull, D.E.S. Optical Imaging and Analysis of Speckle Patterns from Escherichia Coli in Disinfectant Solution. In Proceedings of the CLEO/Europe Conference on Lasers and Electro-Optics, Glasgow, UK, 14–18 September 1998; ISBN 0-7803-4233X. [[CrossRef](#)]
70. Watson, A.; Stewart-Tull, D.E.S.; Parton, R.; Peden, I.; Yeo, A.; Tan, B.K.; Ward, G. Laser inactivation of surfaces and detection of bacteria. In *Particles on Surfaces 9: Detection, Adhesion and Removal*; Mittal, K.L., Ed.; VSP: Leiden, The Netherlands, 2007; pp. 83–94. ISBN 9789067644358.
71. Ramírez-Miquet, E.; Martí-López, L.; Contreras-Alarcón, O.R. Escherichia coli activity characterization using a laser dynamic speckle technique. *Revista Cubana de Física* **2011**, *28*, 1E13–1E17.
72. Murialdo, S.E.; Sendra, G.H.; Passoni, L.I.; Arizaga, R.; Gonzalez, J.F.; Rabal, H.; Trivi, M. Analysis of bacterial chemotactic response using dynamic laser speckle. *J. Biomed. Opt.* **2009**, *14*, 064015. [[CrossRef](#)]

73. Ramírez-Miquet, E.E.; Otero, I.; Rodríguez, D.; Darias, J.G.; Combarro, A.M.; Contreras, O.R. Differences in activity profile of bacterial cultures studied by dynamic speckle patterns. *Proc. SPIE* **2013**, *8587*, 85871P. [[CrossRef](#)]
74. Murialdo, M.E.; Passoni, L.; Guzman, M.N.; Sendra, G.H.; Rabal, H.J.; Trivi, M.R.; Gonzalez, J.F. Discrimination of motile bacteria from filamentous fungi using dynamic speckle. *J. Biomed. Opt.* **2012**, *17*, 056011. [[CrossRef](#)]
75. Balmages, I.; Bliznuks, D.; Liepins, J.; Zolins, S.; Lihachev, A. Laser speckle time-series correlation analysis for bacteria activity detection. *Proc. SPIE* **2020**, *11359*, 113591D. [[CrossRef](#)]
76. Loutfi, H.; Pellen, F.; Jeune, B.L.; Lteif, R.; Kallassy, M.; Brun, G.L.; Abboud, M. Interpretation of the bacterial growth process based on the analysis of the speckle field generated by calibrated scattering media. *Opt. Express* **2020**, *28*, 28648–28655. [[CrossRef](#)]
77. Ulianova, O.; Ulyanov, S.; Zaytsev, S.; Saltykov, Y.; Ulyanov, A.; Feodorova, V. LASCA-imaging of GB-speckles: Application for detection of the gene polymorphism in bacterial model. *Laser Phys. Lett.* **2020**, *17*, 6. [[CrossRef](#)]
78. Ulianova, O.; Ulyanov, S.; Zaytsev, S.; Saltykov, Y.; Ulyanov, A.; Feodorova, V. Could LASCA-imaging of GB-speckles be applied for a high discrimination and typing of pathogenic bacteria? *PLoS ONE* **2021**, *16*, e0245657. [[CrossRef](#)] [[PubMed](#)]
79. Zdunek, A.; Muravsky, L.I.; Frankevych, L.; Konstankiewicz, K. New nondestructive method based on spatial-temporal speckle correlation technique for evaluation of apples quality during shelf-life. *Int. Agrophys.* **2007**, *21*, 305–310.
80. Yoon, J.; Lee, K.R.; Park, Y.K. A simple and rapid method for detecting living microorganisms in food using laser speckle decorrelation. *arXiv* **2016**, arXiv:1603.07343.
81. Braga, R. Challenges to apply the biospeckle laser technique in the field. *Chem. Eng. Trans.* **2017**, *58*, 577–582.
82. Catalano, M.D.; Rivera, F.P.; Braga, R.A. Viability of biospeckle laser in mobile devices. *Optik-Int. J. Light Electron. Opt.* **2019**, *183*, 897–905. [[CrossRef](#)]
83. Alves Braga, J.R. When noise became information: State-of-art in biospeckle laser. *Ciencia Agrotecnol.* **2017**, *41*, 359–366. [[CrossRef](#)]
84. Passoni, I.; Rabal, H.; Meschino, G.; Trivi, M. Probability mapping images in dynamic speckle classification. *Appl. Opt.* **2013**, *52*, 726–733. [[CrossRef](#)]
85. Zhang, Y.; Ceylan Koydemir, H.; Shimogawa, M.M.; Yalcin, S.; Alexander, A.; Liu, T.; Oguz, I.; Huang, Y.; Bai, B.; Yilin Luo, Y.; et al. Motility-based label-free detection of parasites in bodily fluids using holographic speckle analysis and deep learning. *Light Sci. Appl.* **2018**, *7*, 108. [[CrossRef](#)] [[PubMed](#)]
86. Arizaga, R.; Trivi, M.; Rabal, H. Speckle time evolution characterization by the co-occurrence matrix analysis. *Opt. Laser Technol.* **1999**, *31*, 163–169. [[CrossRef](#)]
87. Asadishad, B.; Ghoshal, S.; Tufenkji, N. Method for the direct observation and quantification of survival of bacteria attached to negatively or positively charged surfaces in an aqueous medium. *Environ. Sci. Technol.* **2011**, *45*, 8345–8351. [[CrossRef](#)] [[PubMed](#)]
88. Hermansson, M. The DLVO theory in microbial adhesion. *Colloids Surf. B Biointerfaces* **1999**, *14*, 105–119. [[CrossRef](#)]
89. Christensen, G.D.; Simpson, W.A.; Younger, J.J.; Baddour, L.M.; Barrett, F.F.; Melton, D.M.; Beachey, E.H. Adherence of coagulase-negative staphylococci to plastic tissue culture plates: A quantitative model for the adherence of staphylococci to medical devices. *J. Clin. Microbiol.* **1985**, *22*, 996–1006. [[CrossRef](#)] [[PubMed](#)]